VIBRATIONAL MODES OF THE VIOLIN FAMILY

Colin Gough

School of Physics and Astronomy, University of Birmingham, UK profough@googlemail.com

ABSTRACT

The generic wave-mechanical properties of violin-shaped instruments are described by considering their bodies as simplified, shallow, thin-walled, guitar-shaped, shell structures with the arched plates connected around their edges by the ribs. COMSOL finite element software is used to illustrate the strong dependence of the shapes and frequencies of the low frequency A1, CBR, B1- and B1+ signature modes on the rib coupling strength, the island area between the f-holes, coupling to the internal cavity pressure fluctuations via the Helmholtz f-hole resonance, and the soundpost position and strength. The model illustrates the relationship between the free pate modes and those of the fully assembled instrument. It also identifies the important BI- and BI+ signature modes as normal modes involving the in- and out-of-phase combinations of a bending and breathing mode of the shell, with the breathing component responsible for both the directly and indirectly (via the A0 mode) radiated sound. The model describes the vibrational modes over the whole playing range of the violin and can be used to predict both the admittance at the bridge and the radiated sound.

1. INTRODUCTION

Knowledge of the vibrational modes of the violin has advanced rapidly over the last few years from experimental modal analysis of instruments of widely varying quality, including many fine modern and classic Italian instruments by Stradivari and Guarneri instruments and their contemporaries, notably – notably from modal analysis measurements by Marshall [1], Schleske [2], Bissinger [3] and Stoppani [4]. In addition, several finite element computational investigations have successfully reproduced the shapes and frequencies of many observed vibrational states, including those of Knott [5], Roberts [6], Rogers and Anderson [7], and Bretos et al [8].

Nevertheless, the origin and nature of even the most important A0, CBR, B1- and B1+ signature modes, responsible for almost all the sound radiated below around 800Hz to 1 kHz, has not been clearly understood. This is largely because of the asymmetric and often complicated shapes of the observed and computed modes

This investigation therefore adopts a somewhat different approach to that of previous finite element computa-

Copyright: © 2013 First author et al. This is an open-access article distributed under the terms of the <u>Creative Commons Attribution License 3.0</u> <u>Unported</u>, which permits unrestricted use, distribution, and reproduction in any medium, provided the original author and source are credited.

tions. It aims to explain and elucidate the origin and nature of the important acoustical modes of vibration, rather than simply to predict them for specifically chosen physical parameters related to a particular or typical violin.

To this end, we assume the simplest possible model having the necessary symmetry and constraints to reproduce the vibrational modes of violin-shaped instruments. This can be achieved by describing the hollow shell of such instruments as shallow, thin-walled, arched plate, guitar-shaped boxes, with *f*-holes cut into the top plates and offset soundpost and bass bar. Despite the added simplification of assuming uniform, isotropic, elastic constants and plate thicknesses, the model closely reproduces the frequencies and shapes of the frequencies and shapes of the signature modes of the assembled instrument shapes, and correctly predicts modal densities of anisotropic plates at high frequencies as recognized by Cremer [9, §11.2]

As an aid to such physical understanding, the modes of the instrument are first investigated for a symmetric empty shell without soundpost or bass bar, then with a centrally placed sound post and finally with the symmetry-breaking offset soundpost and bass bar. The symmetry-breaking results in relatively complicated asymmetric modes involving the coupling together of previously symmetric and anti-symmetric modes about the central axis.

The model describes how the modes of the initially free plates are transformed into those of the assembled instrument, as the interactions between the initially free plates by the ribs, the internal cavity pressure fluctuations and the offset soundpost are slowly increased from near zero to typical values.

Although the focus of this paper is on the low frequency signature modes, the shapes and frequencies of the shell modes can be determined over the full playing range of an instrument. The absence of damping in the modal computations circumvents the practical problem of the strong overlap of modal resonances from damping at high frequencies leading to increasingly complex deflection shapes (*ODS*) involving combinations of the previous ideally symmetric and anti-symmetric flexural plate modes.

Nevertheless, damping is easily introduced into the computations. This enables the frequency dependence of the input admittance at the bridge and radiated sound to be derived as a continuous function of frequency over the whole playing range.

As described in this paper, the model enables one to investigate the dependence of important mode frequencies and shapes on the rib strength, plate masses, arching profiles, internal cavity air resonances, and, most importantly, the sound post strength and location. The position of the sound post within the island area relative to the feet of the bridge is shown to have a major influence on both the resonant frequencies of the signature modes and the strength with which they can be excited by the bowed string.

In the following sections, the model is introduced and used to illustrate:

- the transformation of the front and back free plate modes into those of the assembled instrument,
- the identification of the *B1* and *B1*+ signature modes as the coupled vibrations of the component bending and breathing modes of the shell,
- the influence of the *f*-holes on both the internal cavity air pressure vibrations and the coupling of such fluctuations to the shell vibrations which excite them,.
- the dependence of the signature and higher frequency modes on rib strength, the *f*-holes and island area, coupling to the air inside the cavity via the *f*-hole Helmholtz resonance and, most importantly, the soundpost position.

A longer paper will include and quantify the computed influence of elastic anisotropy, the linings and corner/end blocks, arching profiles and plate thicknesses, in addition to the coupled vibrations of the strings, neck and fingerboard and higher-order cavity air modes, as well as a description of the generic properties of the higher frequency modes.

2. FINITE ELEMENT MODEL

The finite element geometry of the violin illustrated in Fig.1 is loosely based on the internal rib outline, arching profiles and other physical dimensions of the Titian Strad (Zygmuntowicz [10]). As we are interested in the vibrational properties of all instruments of the violin family, the exact dimensions and detailed geometry are only of secondary importance. Variations in physical and geometric properties can always be included later as relatively small perturbations, changing specific mode frequencies, but not the symmetry of their underlying shape. The model will be described in detail in a separate publication.

The unmeshed geometric model used for the finite element computations is illustrated in figure 1. The 15 mm high arching profiles of the plates were defined by simple mathematical functions, with identical top and back plate profiles across the width, but slightly different profiles along the length.

For simplicity, plates of uniform thickness have initially been considered, with uniform elastic properties representing the geometric mean of the anisotropic properties along and across the grains. This ensures the correct mode density at high frequencies (Cremer [9, §11.2]). The top and back plate thicknesses (2.5 and 3.5 mm), densities (460 and 660 kg/m³), masses (57 and 118 g) and averaged along/cross-grain elastic constants (2.39 and 2.17 GPa) were chosen to closely reproduce typical

arched front and back plate frequencies, as listed in table

Frequency Hz	#1	#2	#3	#4	#5
Back FEA	93	169	248	252	348
Hutchins	116	167	222	230	349
Front FEA	82	158	218	231	333
Hutchins	80	146	241	251	295
Cremonese		134			314

Table 1. Arched FEA back and front free plate frequencies compared with Hutchins' "tuned" plates (cited from Roberts [6]) and average values for nine Cremonese violins (Curtin [11) both with f-holes in the front plate

The 2.1:1 ratio of the computed top plate #5 and #2 modes is slightly larger than the octave tuning advocated by Hutchins [12], but lower than the average 2.3:1 value for fine Cremonese violins measured by Curtin [11]. However, the values are well within the experimental scatter amongst fine instrument, which justifies the use of the use of the assumed isotropic plate parameters for our subsequent development of the modes of the assembled instrument. The influence of elastic anisotropy and graduations of plate thicknesses on mode shapes and frequencies will be described in a later paper.

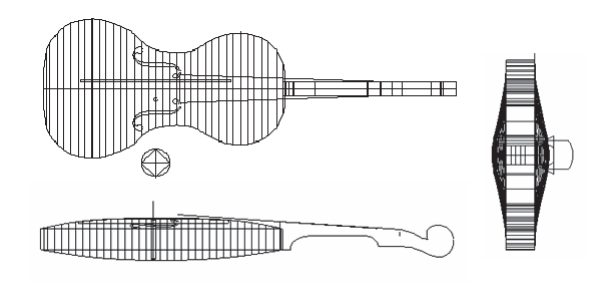


Figure 1. The unmeshed geometric model before meshing used for the finite element computations illustrating the guitar-shaped outline and arching of the plates and schematic representation of the neck. The transverse and longitudinal lines across define the cross-sections along which the arching profiles were defined. The circular disc is used to demonstrate the induced *f*-hole Helmholtz vibrations.

Although the computations presented in this paper are for the violin, the mode shapes and dependencies of modal frequencies on physical and geometric factors are expected to be much the same for instruments of any size, as the symmetry of the mode is largely determined by the symmetry of the shell structure, which is much the same for all instruments of the violin family.

The computations were made using the structural shell module of COMSOL 3.5 Multidisciplinary software. An automated mesh with typically 50,000 degrees of freedom was generated, with the first 20 to100 or so vibrational modes of the freely supported instrument computed in a few tens of seconds on a desk-top PC.

The influence on the vibrational modes of the individual plates, the ribs, *f*-holes, central and offset soundpost, and internal air cavity are now considered in turn. Space

precludes a description of the influence of bass-bar and neck/fingerboard assembly, which perturb but do not significantly influence the generic properties of the vibrational modes of the instrument of main interest her.

3. FREE PLATE MODES

Figure 2 illustrates the computed free plate modes used to model the assembled instrument, before *f*-holes have been cut or bass bar added. Throughout this paper a colour scale will be used to illustrate displacements perpendicular to the plates, with dark red and blue representing equal but opposite displacements perpendicular to the plate, with the nodes at the transition between green and yellow.

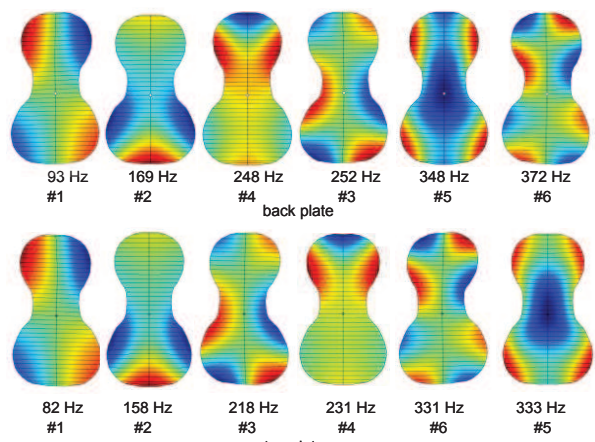


Figure 2. The first six modes of the isotropic, uniform thickness, arched, top and back plates

Arching results in a strong coupling between the flexural waves perpendicular to and longitudinal waves parallel to the arched surfaces. This can double the frequency of the low frequency plate modes, though it is less important as the mode frequencies increase. Such coupling also induces significant in-plane edge contractions and extensions, responsible for the coupling between the bending and breathing modes of the assembled instrument. The plate frequencies are therefore strongly dependent on how they are supported by the ribs both in plane and perpendicular to their edges. Figure 2 demonstrates that even relatively small changes in arching profile along the lengths of the top and back plate can reverse the order of the mode frequencies, even though their arching heights are the same.

The individual modes are either symmetric or antisymmetric about the longitudinal central axis. This remains true for their coupled motions in the assembled instrument in the absence of the symmetry-breaking bass bar and offset soundpost.

Mode #1 is a torsional mode of relatively little acoustic Modes # 2 and #4 involve flexural bending vibrations in the lower and upper bouts of the freely supported plates. Mode #4 is higher in frequency because it is confined to a smaller area. Mode #2 is often referred to as the X-mode, on account of the shape of its nodal lines, though they never cross. As we will show later, the coupled #2 and #4 modes result in the largely non-radiating bending mode component of the B1- and B1+ signature modes. Mode #3 is a higher frequency torsional mode, which includes some bending. Both plates vibrating in the same direction result in the CBR mode of the assembled instrument. Mode #5 is often referred to as the ring-mode on account of the nodal line around the central region of the plate moving in the same direction. When coupled by the ribs, the resulting mode with the two plates vibrating in opposite directions is responsible for the breathing mode components of the BI- and BI+ signature modes. These modes are directly or indirectly (by excitation of the A0 f-hole resonance) responsible for virtually all the sound radiated by the violin and other stringed instruments at frequencies over their first two octaves.

4. RIB COUPLING

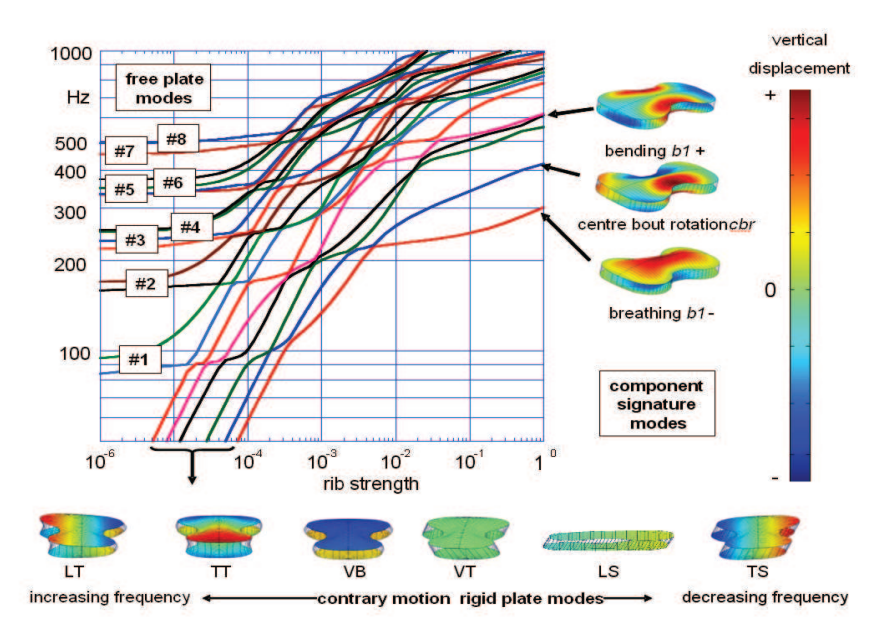


Figure 3. The computed transformation of the first eight modes of the free plates to those of the fully assembled but empty, doubly-arched, guitar-shaped, shell structure without *f*-holes, as a function of rib coupling strength increased from a very small value to that of a typical violin (see text). The mode frequencies are also strongly perturbed by the illustrated contrary rotational and linear vibrations of the rigid plates about their three orthogonal axis, with unperturbed vibrational frequencies proportional to (rib strength)^{1/2}.

Figure 3 illustrates the rather complicated way in which the modes of the individual free plates are transformed into those of the assembled instrument on increasing the rib coupling strength from close to zero to a representative normal value.

The coupling strength is proportional to $E_{rib}(t/h)^3$, where E_{rib} is an effective elastic constant across the ribs of height h and thickness t. In computing the dependence on rib strength the rib height (3 cm) and thickness (1mm) were held constant, while E_{rib} was scaled from a very small value to 10 GPa - a typical value for maple. For the cello, with its significantly larger rib height to thickness ratio, the rib coupling strength will be significantly weaker than that of the violin. This will result in relatively larger stretching and bending of the ribs.

The density was also simultaneously scaled by the same factor to maintain the frequency of the wave-guide like, flexural, rib modes between the two plates at a high frequency, typically >5-10 kHz for the violin and >800 Hz for the cello (Stoppani, private communication) - well above the range of frequencies considered here. At lower frequencies, the ribs simply act as a series of parallel cantilevered springs inhibiting plate separation and bending around their edges. Nevertheless the isolated rib garland can easily be bent and twisted about its length with very little energy. Such vibrations are involved in the *CBR* and BI- and BI+ signature modes of the violin, with large amplitude twisting and bending of the ribs along their edges, but relatively small amounts of stretching and bending between opposing plate edges.

Figure 3 shows that the ribs have a major influence on the frequencies and shapes of the low-lying modes of the assembled shell, which become the signature modes of the fully modeled instrument. The coupling is especially strong between front and back plates sharing the same symmetry and closely spaced frequencies.

As well as the coupled free plate modes, there are six additional modes derived from the twelve zero-frequency degrees of freedom of the two isolated plates describing their rigid body displacements and rotations along and about their three orthogonal symmetry axis.

Six of these modes become the six whole-body displacements and rotations of the assembled instrument. The remaining six modes are transformed into modes with the displacements and rotations of the rigid plates in opposite directions, as illustrated in Figure 3. Because such modes involve the stretching and compression of the ribs, their frequencies increase with rib strength as $\sqrt{E_{ribs}/M_{plates}}$, where M_{plates} will be a mode-specific effective plate mass. Their unperturbed frequencies therefore increase with slope ½, when frequency and rib strength are plotted on logarithmic scales, as in figure 3.

At intermediate coupling strengths, these modes cross and will couple to any of the flexural wave modes of the top and back plates sharing a similar symmetry. This results in considerable veering and splitting of several mode frequencies in the cross-over region. The splitting of modes is proportional to the rib-induced interaction strength. Modes not sharing a common symmetry do not interact. Their frequencies simply cross.

At full coupling strength, the influence of the rigid plate modes are less important but still account for the small amounts of rib stretching, rotations and twisting observed in experimental modal analysis measurements.

Because of these interactions, the dependence of shell mode frequencies on rib strength is rather complicated and difficult to interpret. In figure 5a-d below, we have therefore extracted those parts of the dispersion curves that identify the transformations of specific plate modes to the low frequency modes of the assembled instrument.

Before leaving figure 3, it is important to note that, despite the complexity of the modal frequency plot, the number of modes of the assembled structure is always conserved and is equal number of the number of initially non-interacting modes considered. It is therefore possible to follow a single mode of the interacting system from that of the original uncoupled modes as they adiabatically (smoothly) transformed to those of the fully coupled structure. However, as the coupling strength increases each mode will increasingly include additional coupled component vibrations of the initial system.

As a result of the increase in modal frequencies on increasing rib strength, the number of low frequency modes of the shell at full coupling strength is relatively small. The five lowest modes are illustrated in Figure 4. These will be referred to as the cbr (centre bout rotation), bl- (breathing), bl+ (bending), ld (longitudinal dipole) and td (transverse dipole) modes of the empty shell. Note the use of small letters to denote what become contributing component modes of the CBR, Bl- and Bl+ normal modes of the assembled instrument.

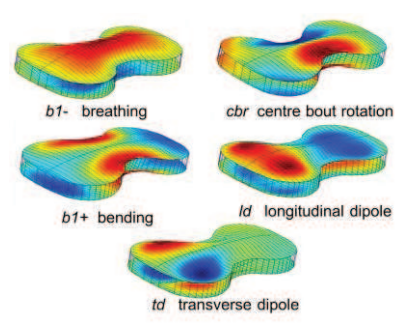


Figure 4. The first five component or basis modes of the assembled guitar-shaped box at full rib-coupling strength.

The transformation of each of the first five free plate modes into the above modes of the freely supported assembled shell will now be described.

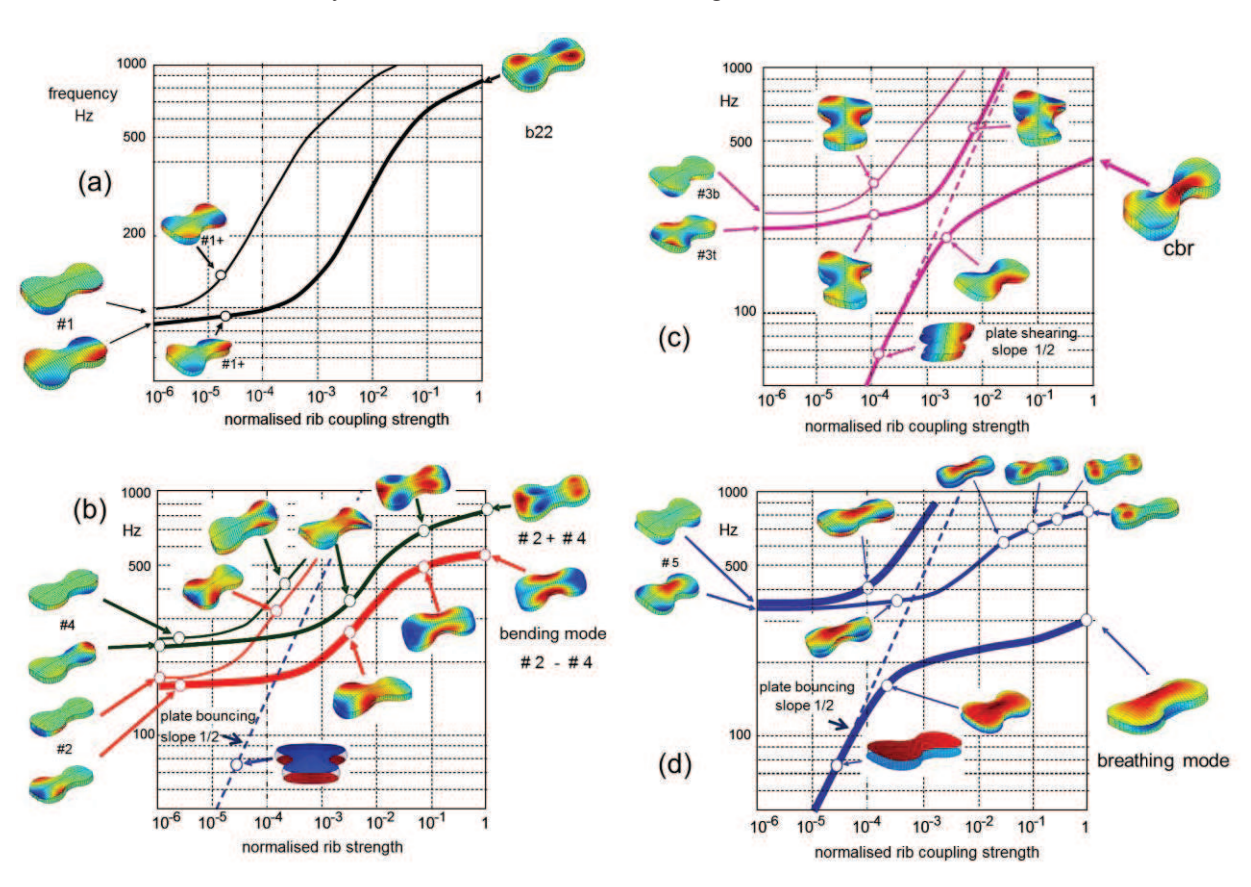
Figure 5a illustrates the influence of rib coupling on the #1 torsional plate mode. Even at vanishingly small coupling, the top and back plates are coupled together to form two new *normal* modes with the plates twisting in either the same or opposite directions. The mode with both plates twisting in the same direction avoids stretching the ribs. Its stored energy, hence frequency, therefore increases far less rapidly with rib coupling strength than the contra-twisting mode, which rapidly rises in frequency into the multiplicity of flexural plate modes above a kHz. The mode with plates twisting in the same direction also transforms into a relatively unimportant acoustic mode just below a kHz.

Figure 5b illustrates a similar initial behaviour for the coupled #2 and #4 free plate modes, with the frequency of the modes with plates flexing in opposite directions increasing much more quickly than when flexing in the same direction, avoiding stretching the ribs. In contrast, the pair of modes with plates vibrating in the same direction are coupled together by the ribs to form the important component, anticlastic (bending in opposite directions), bI+ bending mode of the BI- and BI+ signature modes of the fully instrument.

The #3 modes illustrated in figure 5c behave in much the same way, with plates vibrating in opposite senses increasing rapidly in frequency. However, in this case, the lower frequency mode, with the two plates vibrating in the same direction, crosses and interacts strongly with the more rapidly increasing frequency shearing mode of the rigid plates. After crossing, the emerging cbr mode still describes the centre bout rotation, but retains a significant amount of coupled shearing motion. This results in a central bout rhombohedral distortional vibration, explaining the origin of the CBR name. However, it is its rotation rather than its shear motion that is important in coupling to the rocking bridge. It would therefore arguably be more appropriate to refer to this mode as a centre bout rotation mode. Because such motion involves little change in volume, the cbr mode, which transforms into the CBR mode of the fully assembled instrument, usually only plays a minor role in the radiation of sound.

Figure 5d illustrates the very strong interaction of the #5 plate modes with the rising frequency bouncing mode. Inspection of the resulting mode shapes identifies the lowest and highest frequency branches (the thicker solid line) as the in- and out-of-phase of the coupled #5 "ring-modes" with the rigid plate bouncing mode (involving the stretching and compression of the ribs). The lower mode becomes the all-important component b1breathing mode responsible for almost all the sound radiated directly or indirectly (via its excitation of the fhole Helmholtz resonance) by instruments of the violin family over their lowest two octaves. On crossing the rising bouncing mode frequency, the breathing mode reemerges at a significantly lower frequency than its initial value, as expected for any pair of strongly coupled oscillators. In contrast, the mode with the initial #5 ring plate vibrations in the same phase simply crosses the bouncing mode frequency and becomes another relatively unimportant acoustic mode in the transition region just below 1 kHz.

In every case, the mode frequencies are still rising for a coupling factor of unity corresponding to typical values. This reflects the increasing rigidity of the supporting ribs, which increasingly constrain the bending and stretching of the flexural waves around the plate edges.



Figures 5a-d. Extracted dispersion curves for the transformations of the first five free plate modes to the lowest frequency modes of the assembled shell.

6. f-HOLES AND ISLAND AREA

The open *f*-holes on the front plate and the island area between them play a major role in the sound of the violin and related instruments, as recognized by Cremer [1, chpt.10]. Firstly, the open holes result in the *A0* Helmholtz cavity resonance, which boosts the sound of all members of the violin family over their first octave or so. Secondly, the free *f*-hole edges define the shape of the island area, which strongly influences the penetration of flexural waves from the lower and outer bouts towards the two feet of the rocking bridge, which excite them. As shown later, the penetration of flexural waves into the island area and resulting excitation of radiating modes is also strongly influenced by the strength and position of the soundpost in the island area.

6.1 The island area

Figure 6 illustrates the influence of the *f*-holes on the low frequency flexural wave modes of the shell. The frequencies were computed as a function of *f*-hole strength varied by simultaneously decreasing the elastic constant and density of the *f*-hole areas by the same factor from unity (no *f*-holes) to 10^{-5} (effectively open *f*-holes).

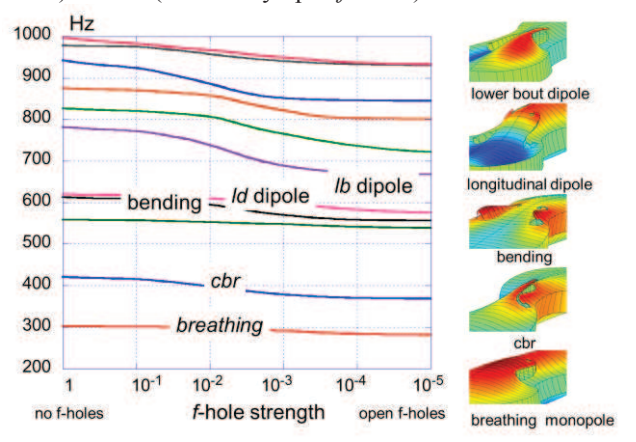


Figure 6. The influence of the *f*-holes on the empty shell mode frequencies and shapes in the island area.

Opening the *f*-holes has little effect on mode shapes, but lowers their frequencies by increasing their penetration into the island area towards the free edges of the island area. As a result the inside edges of the *f*-holes can vibrate with large amplitudes, almost independently from the outer edges constrained by the ribs, as illustrated.

6.2 The Helmholtz A0 resonance.

The combined open area A of the two f-holes together with the volume V of the internal cavity, if rigid, would form a Helmholtz resonator, with resonant frequency

$$2\pi f_{Helmholtz} = c_o \sqrt{gA^{1/2}/V}, \qquad (1)$$

where c_o is the velocity of sound within the cavity and g is an f-hole, shape-dependent, constant of order unity. The resonance is excited by the volume-changing, b1-component of the cavity wall flexural wave vibrations.

Although the Helmholtz frequency, proportional to the velocity of sound in air, is independent of pressure, the strength of the coupling between the induced cavity pressure fluctuations and flexural plate vibrations that excite them is proportional to the ambient pressure. Figure 7 illustrates the dependence of the shell modes and $A0\ f$ -hole frequencies on ambient pressure.

The computations assume a uniform acoustic pressure within the cavity induced by the cavity volume changes. These are computed self-consistently and describe the interaction of the shell wall vibrations with the air inside the cavity via their coupling to the f-hole Helmholtz A0 resonance. For uniform pressure changes, only volume only volume changing shell wall vibrations can provide such coupling.

Figure 7 illustrates the very strong perturbation of the A0 and b1- breathing modes, as the ambient pressure is increased. Neglecting, interaction with the enclosed air is equivalent to zero ambient pressure. The previously computed empty shell breathing mode frequency of around 300 Hz is then very close to that of the modeled ideal Helmholtz resonator at 309 Hz. On increasing the internal pressure to a "normal" value, the coupling is so great that the predicted A0 mode would drop to around 200 Hz, while the breathing mode would be raised to around 400 Hz. Analytic models, based on inertial rather than springlike coupling, provided via the acceleration of the cavity walls and the pressure within the cavity, predict that the product of the resulting a0 and b1- mode frequencies should remain constant, as confirmed by the computations.

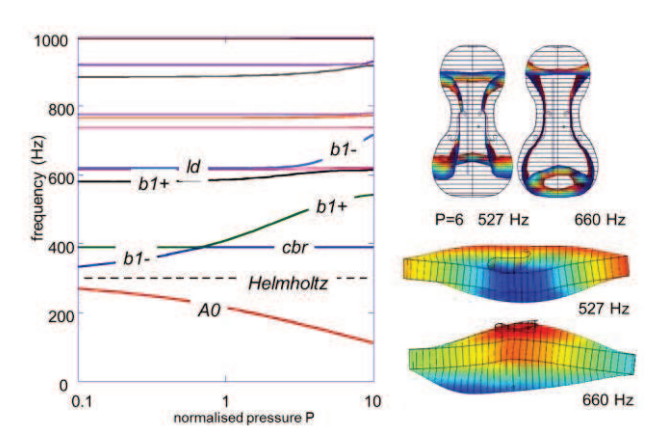


Figure 7. The variation of the low frequency modes of the empty guitar-shaped shell with *f*-holes cut into the top plate, as a function of ambient pressure normalized to normal air pressure. The dashed line indicates the unperturbed Helmholtz frequency of 307 Hz. Also illustrated are the mode shapes and reversed *baseball-like* nodal lines of the coupled *b1*-breathing and *b1*+bending mode at high pressures.

As described in an accompanying paper (Gough [13]), the internal pressure driving the Helmholtz vibrations of the air in and out of the f-holes is reduced below the average pressure - because of the pressure drops associated with flow along the length of the cavity towards the f-holes. This reduces the effective pressure driving the f-hole resonance by a factor of ~ 0.7 , equivalent to reducing the effective ambient pressure by the same factor.

Measurements on violins with and without a soundpost show typical drops in A0 frequency from around 285 to 240 Hz, in qualitative agreement with the above model.

Initially, none of the other modes are significantly affected. However, as the pressure increases, the frequency of the bI- breathing mode approaches and would otherwise cross that of the bI+ bending mode.

Because the bending and breathing modes similar but different amplitude in-plane contractions and extensions around the edges of the plates, they are relatively strongly coupled. They then form what become the dominant BI- and BI+ signature modes of the assembled instrument with bending and breathing component vibrations in either the same or opposite phases, as illustrated in figure 7. This is one of the major results of the present investigation and has been confirmed by modal analysis measurements by Stoppani [invited talk at this conference] on many fine instruments.

The coupling of the bending and breathing modes automatically accounts for the characteristic reversal of the baseball-shaped nodal lines. Previous attempts to describe the BI- and BI+ modes have suggested they involve the reversal of #2 and #5 free plate modes in the top and back plates, despite such modes having very different plate edge displacements. Furthermore, the coupling explains why the BI- and BI+ modes are never coincident. It also explains the variations in relative monopole radiation strengths of such modes, which will depend on the contributing strengths of the component BI- breathing (strongly radiating) and BI+ bending (weakly radiating) modes.

There is also a somewhat smaller interaction with the higher frequency longitudinal dipole mode illustrated in figure 4 and with a higher frequency mode just above 900 Hz.

6. THE SOUNDPOST

The soundpost wedged between the plates acts as a supporting beam exerting equal and opposite forces and couples to the plates across its ends. This imposes almost equal flexural wave plate displacements and slopes across its ends assuming intimate contact between the ends of the sound post and the plates.

As a result, the flexural wave displacements at both ends of the sound post tend to be extremely small. This involves a modification of the flexural mode of the empty shell by the addition of a localised flexural wave decaying exponentially as e^{-kr} at large distances, where $k=2\pi/\lambda$ is given by the usual flexural wave dispersion relationship, $\omega \propto tk^2$ and λ is the characteristic wavelength of the standing waves excited in the upper and lower bouts. The existence of such waves is a characteristic feature of bending waves on thin-walled structures and have to be added to the more familiar wave-like functions at any boundary to satisfy the various boundary conditions involved –around the plate edges, along the f-hole slots and, in this case, at the ends of the soundpost.

When located within the island area, the soundpost then acts as a kind of gate inhibiting the penetration of flexural waves in the lower bout past the sound post into the upper bout and vice versa. Because the flexural wave amplitudes are rather small and vary rapidly close to the soundpost ends, its position relative to the two feet of the bridge which excite the shell vibrations is crucial. The strength with which any vibrational mode of the shell can be excited by a horizontal bowing force at the bridge is critically dependent on the wave amplitudes at the two feet of the bridge, which excite such vibrations. The crucial role of the soundpost on the sound of an instrument is why the English call it the soundpost, while the French and Italians more imaginatively refer to it is as the soul and spirit of the instrument.

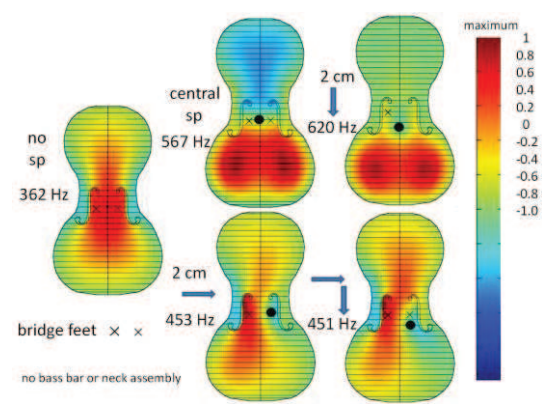


Figure 8. An overview of the influence of soundpost position on the frequencies and top plate mode shapes of the *b1*- breathing mode, for the empty shell without bass bar or other attachments, but coupled to the internal air via the *f*-hole resonance. Modes are illustrated for the empty shell, a centrally placed soundpost, when it is shifted longitudinally and transversely separately by 2 cm, and when shifted in both directions together.

The gate-like function of the soundpost is evident from Figure 8. Without a soundpost, the breathing mode extends through the island area to both upper and lower bouts, with the strongest amplitudes at the upper end of the lower bout and within the island area. Because there is little restriction on the area available for the waves, the frequency is relatively low. In contrast, the nodal regions created by the centrally placed sound post strongly inhibits the penetration of waves from the lower to the upper bout, though there is still some penetration on both sides of the soundpost resulting in weak displacement of opposite sign in the upper bouts. Because of the restriction on available area for the lower bout vibrations, the frequency of the mode is increased very significantly from 362 to 567 Hz. Displacing the soundpost 2 cm towards the lower bouts further inhibits penetration past the sound post and the area available for vibrations is decreased, resulting in a further increase in mode frequency from 567 to 620 Hz. Because all the above modes are symmetric about the central axis, they cannot be excited by a horizontal force causing a symmetric rocking of the bridge. The violin would radiate very little sound.

Moving the soundpost 2 cm sideways from its central position has two affects. It allows the lower bout waves to penetrate more easily through the bass side of the island area, significantly lowering the mode frequency from 567 to 453 Hz. The sideways displacement also introduces a large asymmetry of the wave motion across the two feet

of the bridge. A horizontal bowing force can then couple strongly to the modes via the asymmetrically rocking bridge and hence radiate strongly. Because the waves already penetrate relatively easily past the offset sound post, moving it further away from the bridge results in a relatively small change in mode frequency from 453 to 451 Hz, though it results in quite a large change in the wave motion within the island area and upper bouts, particularly in the region of the two bridge feet.

Although such displacements are very much larger than the mm or so used by violin makers when setting up a violin, the computations illustrate how such changes are likely to change the sound of an instrument, both by changing the frequency of the important breathing mode component and the strength with which it can be excited by horizontal bowing forces at the bridge.

In view of the relatively large variations in *B1*- and *B1*+ signature mode frequencies and their component breathing mode responsible for the radiated sound, even amongst many fine Cremonese instruments, it is somewhat surprising that many luthier's believe there is a "correct" position for the soundpost within a mm or so of its placing relative to the treble side foot of the bridge. This may well be true for fine instruments with properties already optimized for the "correct" soundpost position. But one has to ask why use is not made of the sensitivity of sound quality on soundpost position to "improve" the sound of poorer quality violins by much more adventurous shifts than the mm or so usually considered.

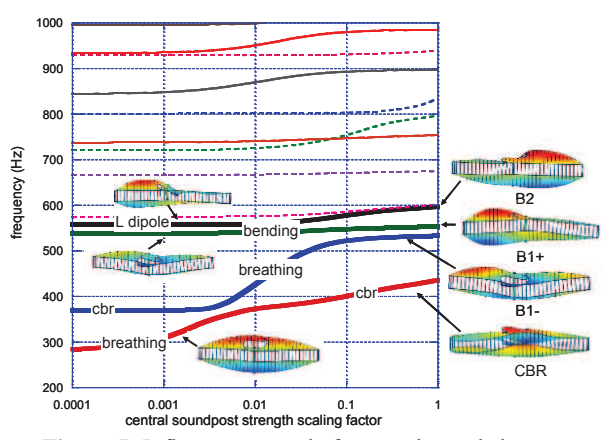


Figure 7. Influence on mode frequencies and shapes of the strength of a centrally placed soundpost.

Figure 7 illustrates the dependence of mode frequencies on the strength of a centrally placed soundpost in-line with the f-hole notches, for the violin body shell without bass bar, fingerboard/neck assembly and neglecting coupling to the Helmholtz cavity resonance. As with the ribs, the soundpost strength is varied by simultaneously increasing its elastic constant and density to maintain its resonant modes at a high value - above \sim 5 kHz for the violin, to avoid complications from the multiplicity of soundpost modes for small elastic constants. A centrally placed soundpost only significantly perturbs symmetric shell modes.

As already illustrated above, the most important feature is the strong increase in frequency of the *b1*- breathing mode. This first crosses the frequency of the *cbr*

mode with a small amount of veering and splitting of mode frequencies indicating an inherent coupling between the bending and cbr mode. The frequency then continues to rise, approaching and otherwise crossing the initially higher frequency b1+ bending mode. In the cross-over region one again observes the formation of the B1- and B1+ modes observed on increasing the internal cavity pressure.

Figure 8 illustrates the strong dependence of the low frequency mode frequencies and interactions on shifting the soundpost along the central axis. By shifting the sound post over relatively large distance both below and above the central bridge position, one can identify separate noninteracting lower and upper bout breathing modes, which cross without any significant veering or splitting, both of which are coupled to the bending mode, which is scarcely affected by soundpost position. As the centrally placed soundpost is moved along the length, the lower and upper bout breathing mode frequencies change in opposite directions, as the areas in which they are constrained to vibrate increase and decrease. At a given position - about a cm behind the bridge, their frequencies would coincide. However, close to the bridge the lower bout breathing mode is lower in frequency than the upper bout mode,

For the violin, only the BI- and BI+ and sometimes the CBR modes radiate strongly in the monopole signature mode regime, though B2 and other higher frequency modes can introduce additional weak resonant features.

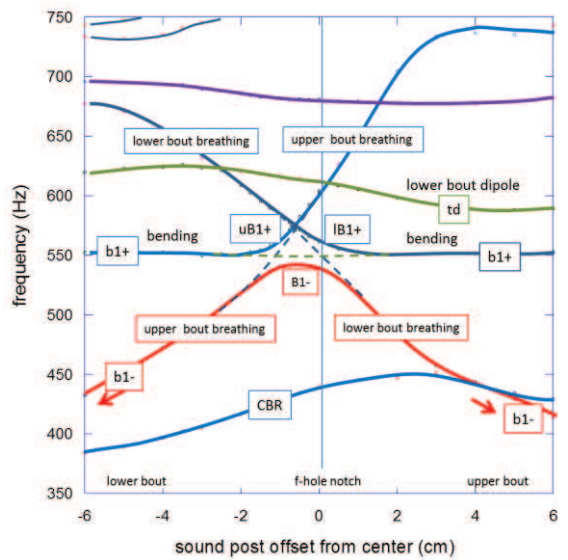


Figure 8. Influence on mode frequencies of shifting the soundpost along the central axis.

The influence on the frequencies of the low-lying modes, on displacing the initially centrally placed sound post away from the central axis is illustrated in figure 9. As described above, this results in a significant decrease in the breathing mode frequency, but only has a small influence on the bending mode. However, as the *b1*- breathing mode frequency crosses the *cbr* mode there is a significant veering of the modes describing their coupled vibrations, implying quite a strong coupling between them.

At present, the physical origin of the coupling involved between the breathing and *cbr* component modes is not understood, but is likely to be a factor in determining why the *CBR* mode of the assembled instrument makes a significant contribution to the radiated sound in some instruments, but not in others.

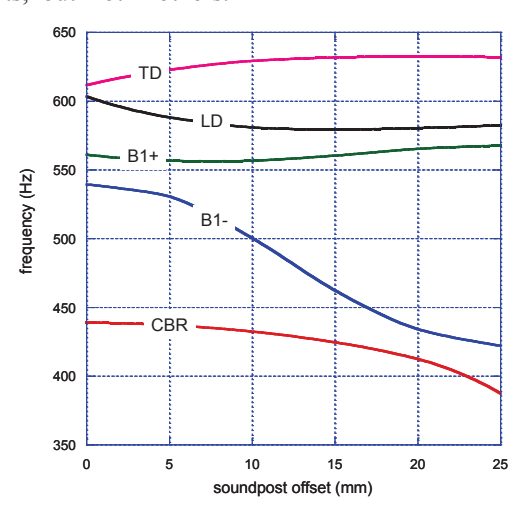


Figure 9. The influence of offsetting a centrally placed sound post from the central axis.

The added influence of anisotropy, bass bar, fingerboard-neck assembly and coupled air modes will be described in a later paper, but do not significantly change the predictions symmetries and coupling interactions in any significant way.

8.SUMMARY

A wave mechanical model to describe and explain the vibrational modes of all members of the violin family has been introduced. The model is based on finite element computer simulations of the generic properties of the modes of vibration of thin-walled, doubly-arched, guitar shaped, shallow, box-like shell structures. The connection of such modes to the free plate modes had been demonstrated, in addition to their dependence on rib-coupling, the *f*-holes, Helmholtz cavity resonance, and sound post strength and position.

9. REFERENCES

- [1] K.D. Marshall, Modal analysis of a violin, *J. Acoust. Soc. Am.*, vol.77, no.2, 1985, pp. 695-709.
- [2] M. Schleske, "On making Tonal Copies of a Violin" CAS Journal Vol.3, No.2, (Series II), November 1996, pp. 18-28.
- [3] G. Bissinger, Structural acoustics of good and bad violins, *J. Acoust. Soc. Am.*, Vol. 124, No. 3, 2008, pp. 1764-1773.
- [4] G. Stoppani, invited paper at this conference.
- [5] G.A. Knott, A modal analysis of the violin, MSc Thesis, Naval Postgrad. School, Monterey, pp 507-550, in Research Papers in Violin Acoustic 1975-1993 (ed. C.M Hutchins and V. Benade), Acoust. Soc. Am., 1997.

- [6] G.W. Roberts, Finite element analysis of the violin (PhD Thesis, Cardiff,), pp. 575-590 in Research Papers in Violin Acoustic 1975-1993 (ed. C.M Hutchins and V. Benade), Acoust. Soc. Am., 1997.
- [7] O. Rogers and P. Anderson, Finite element analysis of a violin corpus, CASJ, Vol.4., no.4. (Series II), November 2001, pp. 43-49.
- [8] J. Bretos, C. Santamaria and J.A. Moral, Vibration patterns and frequency responses of the free plates and box of a violin obtained by finite element analysis, *Jnl. Acoust. Soc. Am.*, vol. 105, no.3, 1999, pp.1942-1950.
- [9] L. Cremer, The Physics of the Violin, MIT, 1984
- [10] S. Zygmuntowicz, The Titian Strad, *The Strad*, February, 2009, pp 30-34.
- [11] J. Curtin, Tap tones and weights of old Italian violin tops, *Jnl. Violin. Soc. Am.*, Vol 20, no.2, 2006, pp. 161-174.
- [12] C.M. Hutchins, The acoustics of violin plates, Sci. Am., October 1981,pp170-186
- [13] C. Gough, Acoustic characterization of violin family signature modes by internal cavity measurements (contributed paper at this conference).